Voltage-gated transient outward currents in neurons with different firing patterns in rat superior colliculus

Yasuhiko Saito and Tadashi Isa

Department of Integrative Physiology, National Institute for Physiological Sciences, Myodaiji, Okazaki 444-8585, Japan

(Received 10 April 2000; accepted after revision 28 June 2000)

1. We investigated the electrophysiological properties of transient outward currents (TOCs) in neurons with different firing patterns, regular-spiking, fast-spiking and late-spiking neurons, in the intermediate layer (SGI) of the superior colliculus using the whole-cell patch clamp technique in slice preparations obtained from young rats (post-natal days 17–22).

2. Analysis of inactivation kinetics and normalized amplitude revealed that TOCs in regular- and fast-spiking neurons had fast inactivation kinetics (decay time constants (mean ± S.E.M.) of 13·8 ± 1·5 and 11·4 ± 1·2 ms, respectively) and low current densities (36·6 ± 3·3 and 32·1 ± 4·9 pA pF^{-1}, respectively). TOCs in late-spiking neurons, on the other hand, displayed a wide range of both inactivation kinetics (36·7 ± 2·4 ms, with a range from 11·3 to 147·8 ms) and current density (54·0 ± 2·9 pA pF^{-1}, with a range from 9·8 to 131·2 pA pF^{-1}).

3. In regular-, fast- and late-spiking neurons having TOCs with slow time constants (> 50 ms, class II late-spiking neurons), the TOCs were sensitive to 4-aminopyridine (4-AP), with IC_{50} values of 2·9, 2·4 and 1·2 mM, respectively. In late-spiking neurons having TOCs with fast decay time constants (< 30 ms, class I late-spiking neurons), the TOCs were composed of at least two 4-AP-sensitive components (IC_{50} values of 0·2 μM and 3·6 mM).

4. Class I late-spiking neurons displayed non-inactivating outward currents which were highly sensitive to 4-AP. They changed their firing patterns to the regular-spiking mode, not only in response to low concentrations of 4-AP (< 50 μM), but also in response to dendrotoxin (200 nM), suggesting that non-inactivating outward currents contribute to the late-spiking property. However, the components of TOCs which were highly sensitive to 4-AP were also sensitive to dendrotoxin. These results suggest that both or either of the two currents contribute to the late-spiking property of class I late-spiking neurons.

5. Although class II late-spiking neurons also displayed non-inactivating outward currents, the late-spiking property was not abolished by low concentrations of 4-AP and dendrotoxin. They changed to a regular firing pattern in response to a high concentration of 4-AP (5 mM), suggesting that TOCs contribute to late-spiking property of class II late-spiking neurons.

6. The results suggest that TOCs with different properties contribute to the different firing patterns of SGI neurons.

The central nervous system (CNS) includes various types of neurons with different firing responses to depolarizing current pulses (McCormick *et al.* 1985; Connors & Gutnick, 1990). The difference in firing patterns is caused by activation of different sorts of ionic conductances (Llinás, 1988; Baxter & Byrne, 1991; Hille, 1992). Since the temporal pattern of action potentials determines the input–output relationships of the neural circuits, understanding how individual ionic conductances regulate the firing patterns of the neuron is essential in defining the role of individual neurons as elements in the neural circuits.

The ionic conductances (ionic currents) that play major roles in determining the electrophysiological properties include voltage-gated transient outward currents (A-type currents or TOCs). TOCs are potassium currents evoked by depolarizing step pulses from hyperpolarized membrane potentials and show fast activation and inactivation kinetics (Connor & Stevens, 1971; for reviews see Rogawski, 1985; Rudy, 1988; Hille, 1992). Their unique properties indicate that TOCs contribute to regulation of the width of an action potential and its frequency, and to firing patterns (Connor & Stevens, 1971; Segal *et al.* 1984; Gean & Shinick-Gallagher,

1989; Hille, 1992). It has been reported that there are various types of TOCs with different kinetics and voltage dependence of activation and inactivation (Serrano & Getting, 1989; Surmeier *et al.* 1989; Ficker & Heinemann, 1992; Banks *et al.* 1996; Fujino *et al.* 1997). Recent molecular cloning of subunit cDNAs and expression studies have revealed the diversity of potassium channels which give rise to TOCs (for reviews see Pongs, 1992; Chandy & Gutman, 1995; Dolly & Parcej, 1996). Although the diversity of the physiological and molecular characteristics of TOCs has been recognized, it has been unclear whether different types of TOCs contribute to the difference in firing patterns of the CNS neurons.

In the present study, we investigated the properties of TOCs in neurons with different firing patterns in the intermediate layer (SGI) of the rat superior colliculus (SC). Our previous study showed that neurons in the SGI can be classified into at least five subclasses with different firing responses to depolarizing current pulses, each of which may contribute to the functional motor output from the SC (Saito & Isa, 1999). Among them, the three major neuron types, classified as regular-, fast- and late-spiking neurons, were analysed to clarify the relationship between firing patterns and TOCs using the whole-cell patch clamp technique in slice preparations. The three firing patterns have been described in other regions of the central nervous system (Schwartzkroin & Mathers, 1978; McCormick *et al.* 1985; Yarom *et al.* 1985; Dekin *et al.* 1987; Connors & Gutnick, 1990; Kang & Kitai, 1990; Han *et al.* 1993; Kawaguchi, 1995; Fujino *et al.* 1997). We found that TOCs in the three neuron types showed different inactivation kinetics, voltage dependence and sensitivity to 4-aminopyridine (4-AP). Our results indicate that the different firing patterns of the SGI neurons are partially determined by the different properties of TOCs. Some of the data have been presented in an abstract form (Saito & Isa, 1998).

METHODS

Frontal slices of the SC (200–250 μm in thickness) were obtained from young Wistar rats (17–22 postnatal days) using procedures similar to those described previously (Isa *et al.* 1998; Saito & Isa, 1999). In brief, the brain was quickly removed after decapitation under ether anaesthesia. Adequate anaesthesia was judged according to the absence of reflexes to toe pinches. The brain was submerged before and during preparation of the slices in ice-cold sucrose Ringer solution containing (mM): 220 sucrose, 10 NaCl, 2·5 KCl, 10 $MgSO_4$, 0·5 $CaCl_2$, 5 Hepes, and 11 glucose, and bubbled with 100% O_2. Frontal slices of the SC were cut using a Microslicer (DTK-2000, Dosaka EM, Kyoto, Japan) and then incubated in oxygenated standard Ringer solution containing (mM): 145 NaCl, 2·5 KCl, 2 $CaCl_2$, 1 $MgCl_2$, 5 Hepes, and 10 glucose, for more than 1 h before the recording. Whole-cell patch clamp recordings were obtained from neurons selected in the SGI. Patch pipettes were filled with an internal solution containing (mM): 140 potassium gluconate, 20 KCl, 0·2 EGTA, 2 $MgCl_2$, 2 Na_2ATP, 10 Hepes, and 0·1 spermine (pH 7·3). Biocytin (5 mg ml^{-1}) was added to the internal solution to verify the location of recorded neurons. The resistance of the recording pipettes was 2–5 MΩ in the bath solution. The liquid junction potential between the patch pipette solution and the standard Ringer solution was estimated to be −10 mV, and the data were corrected for this voltage. Whole-cell currents and membrane potentials were recorded by an EPC-7 patch-clamp amplifier (List, Darmstadt, Germany). Series resistance was less than 25 MΩ and was routinely compensated by 50–70%. If the series resistance changed by more than 10% of the initial value during recording, the recording was terminated or the data were discarded. Voltage and current signals were filtered at 3 kHz and digitized at 4–200 kHz. All recordings were performed at room temperature (20–24 °C). Data were acquired using a pCLAMP6 hardware/software system (Axon Instruments). Off-line analysis was performed with Axograph software (Axon Instruments).

Recordings of the firing patterns were made in the oxygenated standard Ringer solution described above. TOCs were recorded in control solution containing (mM): 115 NaCl, 2·5 KCl, 2·8 $MgCl_2$, 5 Hepes, 10 glucose, and 35 *N*-methyl-D-glucamine (NMG). To eliminate Na^+ currents, we added 0·25 μM tetrodotoxin (TTX) to the control solution. Since Ca^{2+} currents were not easily eliminated, even in the Ca^{2+}-free control solution in slice preparations, we added 0·2 mM $CdCl_2$ to the control solution. When tetraethylammonium chloride (TEA), 4-aminopyridine (4-AP), and high concentrations of KCl were added to the solution, an equimolar concentration of NMG was replaced with them. Neurons with resting membrane potentials more negative than −50 mV and exhibiting overshooting action potentials were used for further analysis of firing patterns and TOCs. The membrane capacitance was estimated from a transient capacitance current in response to a −10 mV hyperpolarizing voltage step from a holding potential of −70 mV. The firing patterns of neurons were examined by application of depolarizing current pulses routinely from two different levels of membrane potential (between −70 and −55 mV and < −75 mV). Except for TTX (Sankyo, Tokyo, Japan), 4-AP and biocytin (Sigma), and dendrotoxin (Alomone Labs, Jerusalem, Isreal), all drugs were purchased from Wako Pure Chemical (Osaka, Japan).

All values are shown as the means ± S.E.M. and error bars in the figures represent the S.E.M. Statistical significance was examined using Student's *t* test (unpaired data) or a one-way ANOVA with a *post hoc* Bonferroni/Dunn multiple comparisons test. Significance was accepted at $P < 0·05$.

The procedures on animals followed the guide for animal experimentation approved by the Animal Research Committee of the National Institute for Physiological Sciences.

RESULTS

Quantitative criteria for classification of three firing patterns

The firing patterns in the three neuron types are exemplified in Fig. 1*A*–*C*. Regular-spiking neurons (Fig. 1*A*) exhibited repetitive firing with relatively constant interspike intervals and moderate spike frequency adaptation. An interspike interval was never more than double the preceding one. Injection of extremely strong current pulses, however, sometimes elicited an increase in spike width and a decrease in the amplitude of action potentials, leading to a blockade of the spike train (data not shown). Fast-spiking neurons (Fig. 1*B*) sustained high-frequency repetitive firing throughout the depolarizing current pulse with virtually no spike frequency adaptation. Late-spiking neurons exhibited

a marked delay in the generation of the first spike due to a transient hyperpolarization that occurred following the onset of the membrane depolarization (Fig. 1*C*, arrow). When the stronger current pulses were applied, the first spike was generated with no delay but a long interval was observed between the first and second spikes (Fig. 1*C*, middle and lower sweeps). This late-spiking property could be observed when depolarizing current pulses were applied at a hyperpolarized membrane potential. When the pulses were applied at a depolarized membrane potential (usually more than −60 mV), late-spiking neurons showed a regular-spiking property (data not shown; see Saito & Isa, 1999).

To clarify and compare the properties of TOCs among neurons with different firing properties, we first determined quantitative criteria for classification of the neuron types, as well as the qualitative differences in firing patterns described in our previous study (Saito & Isa, 1999).

Quantitatively, late-spiking neurons could be well characterized by analysis of the ratio of the interspike interval between the first and second spikes (1st ISI) to that between the second spike and the third (2nd ISI). The interspike intervals in neurons exhibiting delayed spike generation were measured from a spike train obtained by injection of currents adjusted manually to just above the threshold of the first spike generation with no long delay (see Fig. 1*D* insets). The intervals in other neurons were measured from spike trains obtained by injection of currents adjusted to reach an amplitude of depolarization ($V_m = 49{\cdot}7 \pm 0{\cdot}7$ mV, $n = 45$) comparable to those in neurons showing a delayed spike generation ($V_m = 52{\cdot}3 \pm 1{\cdot}1$ mV, $n = 42$) ($P > 0{\cdot}1$, t test, Fig. 1*D*). The amplitude of depolarization, from which the spike amplitude was excluded, was measured from the membrane potential once it had reached a plateau, usually more than 300 ms after the onset of current pulses. Plots of the amplitude of

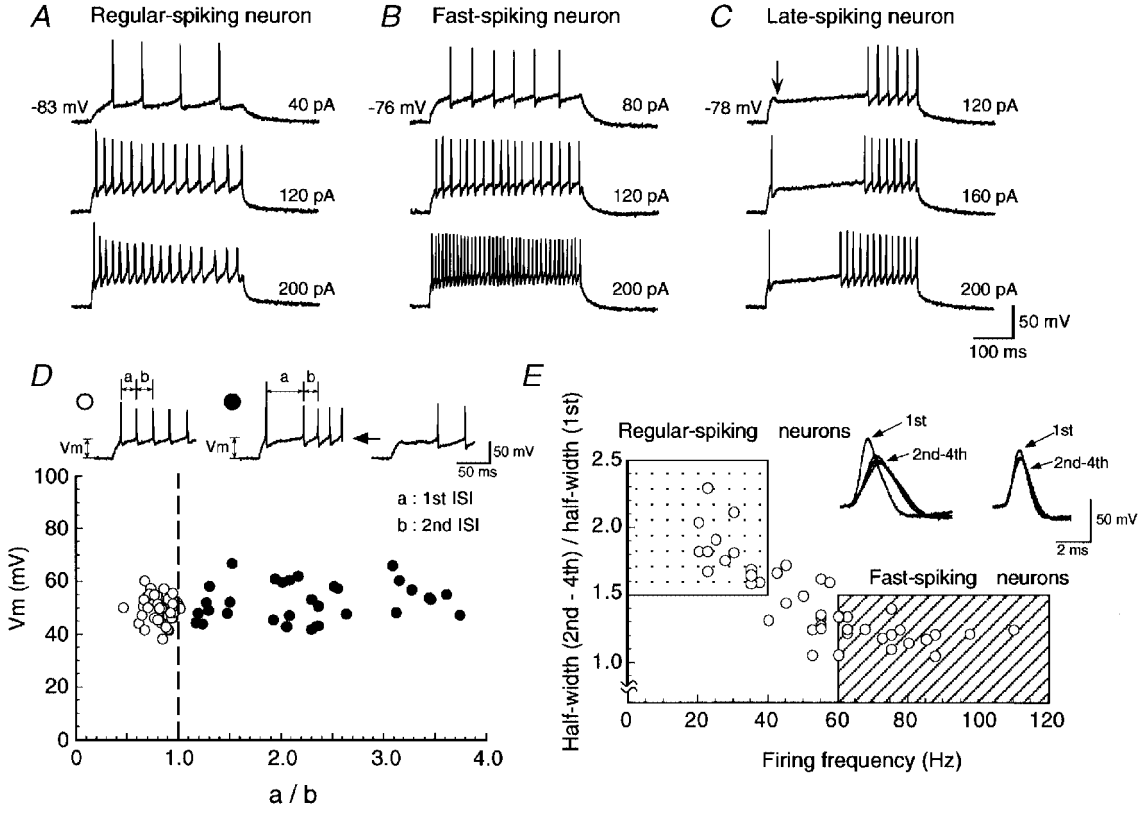

Figure 1. Firing patterns of three neuron types in the SGI of the SC

A–C, firing patterns of regular-, fast- and late-spiking neurons, respectively. Intensities of injected currents are indicated on the right. Note that a transient hyperpolarization occurred following the onset of the membrane depolarization in the late-spiking neuron (*C*, arrow). *D*, the amplitude of depolarization excluding the spike amplitude was plotted as a function of the ratio of the 1st ISI (*a* in insets) to the 2nd ISI (*b* in insets). Filled and open symbols denote neurons with the late-spiking property and the others, respectively (see insets). There was no significant difference in membrane potentials before injection of depolarized current pulses between neurons with late-spiking properties ($-89{\cdot}3 \pm 0{\cdot}6$ mV, $n = 42$) and other neurons ($-88{\cdot}6 \pm 0{\cdot}7$ mV, $n = 45$) ($P > 0{\cdot}1$, t test). *E*, the normalized mean half-width was plotted as a function of the firing frequency. The mean membrane potential before injection of depolarized current pulses was $-88{\cdot}6 \pm 0{\cdot}7$ mV ($n = 45$). In subsequent analysis, neurons located in the dotted area were regarded as regular-spiking neurons (see left inset) and those in the hatched area as fast-spiking neurons (see right inset).

depolarization (V_m) against the ratio of the 1st ISI to the 2nd ISI (a/b), obtained as described above, revealed that the ratios were larger than 1·0 in neurons with a delayed spike generation (filled symbols in Fig. 1*D*), and 1·0 or smaller in other neurons (open symbols in Fig. 1*D*). Therefore, the ratio of the 1st ISI to the 2nd ISI allowed us to discriminate the late-spiking neurons from the others and was used to determine whether a recorded neuron displayed late-spiking properties (see Fig. 6).

To determine whether the recorded neurons were regular-spiking and fast-spiking neurons, we analysed their spike width and firing frequency. The width of individual action potentials was analysed from the spike trains obtained by application of current pulses whose intensity was adjusted to evoke four action potentials in a time window of 80 ms from the onset of current pulses (Fig. 1*E* insets). The firing frequency was measured from a spike train in response to a depolarization of 40–50 mV (47·6 ± 0·7 mV, $n = 45$), because in some of the regular-spiking neurons, application of strong current pulses which induced depolarizations larger than 50 mV caused blockade of spike train. Figure 1*E* shows plots of the normalized mean half-width, obtained from the mean half-width of the second to the fourth spikes divided by that of the first spike, as a function of the firing frequency. To clarify the difference in the firing patterns between regular-and fast-spiking neurons in the present study, we identified neurons with a firing frequency higher than 60 Hz at 40–50 mV of depolarization and a normalized mean half-width smaller than 1·5 (Fig. 1*E*, hatched area) as fast-spiking neurons and analysed the properties of the TOCs. Neurons with a firing frequency lower than 40 Hz and a normalized mean half-width larger than 1·5 (Fig. 1*E*, dotted area), on the other hand, were identified as regular-spiking neurons. The neurons with an intermediate firing frequency (40–60 Hz) were discarded from the analysis in the present study. It was noted that neurons regarded as fast-spiking usually displayed high-frequency repetitive firing (more than 100 Hz) when stronger current pulses were applied. On the other hand, in neurons regarded as regular-spiking high-frequency firing did not occur, even when stronger current pulses were applied.

The approximate threshold for generation of the first spike was estimated for each neuron type and the values were −43·8 ± 1·3, −47·6 ± 1·2 and −45·3 ± 0·8 mV in regular- ($n = 17$), fast- ($n = 28$) and late-spiking neurons ($n = 42$), respectively. The threshold was not significantly different among neuron types ($P > 0·1$, ANOVA *post hoc* test).

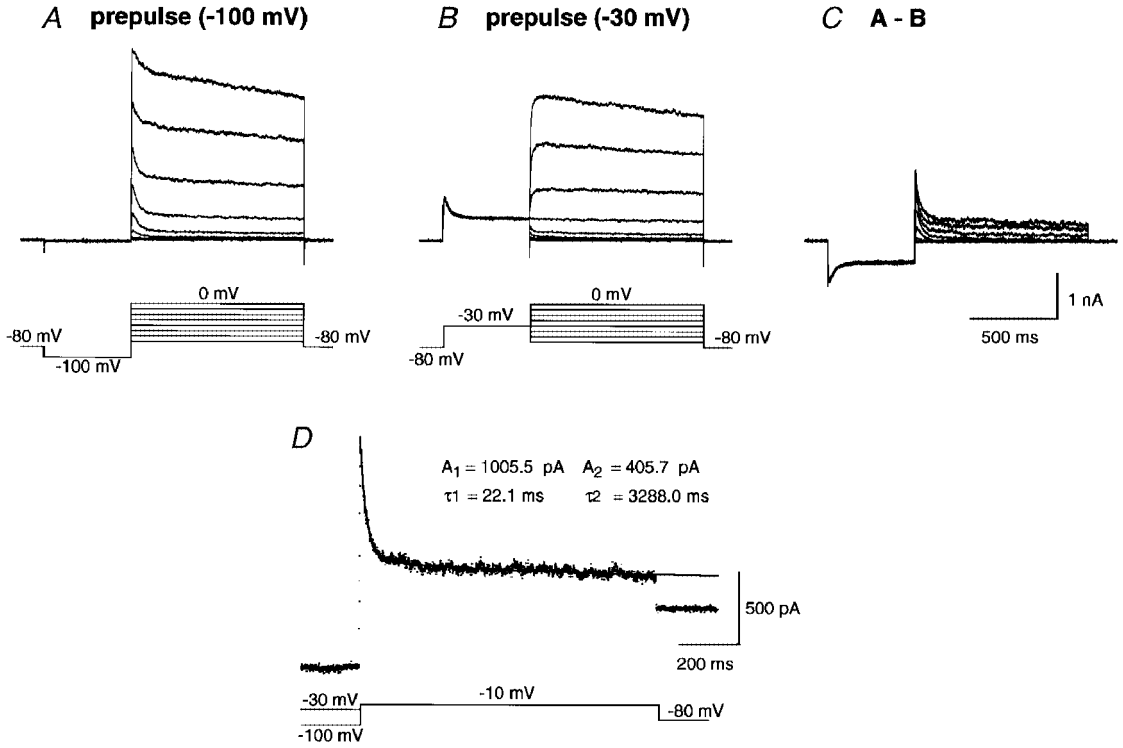

Figure 2. TOCs isolated by the subtraction protocol

A, whole-cell currents (upper traces) evoked by application of a series of depolarizing voltage steps with 10 mV intervals (lower traces) to a neuron following a 500 ms prepulse to −100 mV. *B*, sustained outward currents evoked by application of the same depolarizing voltage steps as in *A* following a prepulse to −30 mV. *C*, isolated TOCs obtained by subtraction of the traces shown in *B* from those shown in *A*. *D*, the decay phase of a current trace obtained by the subtraction protocol was fitted by the sum of two exponential functions. Double-exponential fits are superimposed on the decay phase of a TOC depicted by the dotted trace.

A total of 91 regular-spiking, 72 fast-spiking and 217 late-spiking neurons were classified according to the criteria described above and the properties of TOCs in these neurons were analysed.

Isolation of TOCs from total outward currents

The following conventional subtraction protocol was used to isolate TOCs from total outward currents throughout the present study. In the presence of 0·25 μM TTX and 0·2 mM Cd^{2+}, the application of a series of depolarizing voltage steps (test pulse) with 10 mV intervals following a 500 ms prepulse to −100 mV evoked outward currents which consisted of inactivating and non-inactivating components (Fig. 2*A*). When the depolarizing voltage steps were applied following a 500 ms prepulse to −30 mV, only non- or slowly inactivating outward currents were evoked (Fig. 2*B*). Subtraction of the outward currents evoked by a prepulse to −30 mV from those evoked by a prepulse to −100 mV isolated TOCs from total outward currents (Fig. 2*C*). The decay phase of the TOCs was fitted by the sum of two exponential functions (Fig. 2*D*):

$$I(t) = A_1\exp(-t/\tau_1) + A_2\exp(-t/\tau_2),$$

where A_1 and A_2 are amplitudes obtained from the beginning of the fit range, and τ_1 and τ_2 are decay time constants ($\tau_1 < \tau_2$), indicating the possibility that TOCs are composed of at least two components. The exponential fits were adapted to the decay phase of the TOCs, from the peak to the end of the pulse. Since the component with the faster inactivation turned out to be the major component of the TOCs (see below), we analysed it in order to characterize the properties of TOCs of individual cells with different firing patterns.

The reversal potentials of TOCs were analysed from tail currents evoked by short depolarizing pulses (10 ms) in 7·5 mM extracellular K^+. The mean value of −76·8 ± 0·7 mV ($n = 3$) was comparable with the value predicted from the Nernst equation (−77·1 mV), suggesting that K^+ is the ionic basis of TOCs (data not shown).

Inactivation kinetics and amplitude of TOCs in the three subclasses of neurons

First, in order to characterize TOCs in the three subclasses of neurons, we analysed the inactivation kinetics and the current density of the TOCs. The analysis was carried out from TOCs obtained by subtraction of recordings evoked by application of a voltage pulse from −30 mV to −10 mV from those evoked by a voltage pulse from −100 mV to −10 mV. Figure 3*A–D* exemplifies TOCs induced by the test pulse and exponential fits to the decay phase of the TOCs. The amplitude of the fast-inactivating component (A_1) of TOCs induced by the test pulse to −10 mV was about 70% of the total subtracted outward current (69·1 ± 4·0% in regular-spiking neurons ($n = 31$), 64·7 ± 4·9% in fast-spiking neurons ($n = 19$) and 70·2 ± 1·7% in late-spiking neurons ($n = 83$)). Plots of the current density obtained from the current amplitude (A_1) divided by the whole-cell membrane capacitance as a function of the fast decay time constant (τ_1) (Fig. 3*E*) revealed that TOCs in regular-spiking ($n = 31$, ○) and fast-spiking neurons ($n = 19$, ●) showed fast inactivation kinetics (13·8 ± 1·5 ms, with a range from 6·2 to 43·4 ms, in regular-spiking neurons and 11·4 ± 1·2 ms, with a range from 5·5 to 28·2 ms, in fast-spiking neurons) with small current density (36·6 ± 3·3 pA pF^{-1}, with a range from 5·6 to 78·7 pA pF^{-1}, in regular-spiking neurons, and 32·1 ± 4·9 pA pF^{-1}, with a range from 6·1 to 75·9 pA pF^{-1}, in fast-spiking neurons). There was no

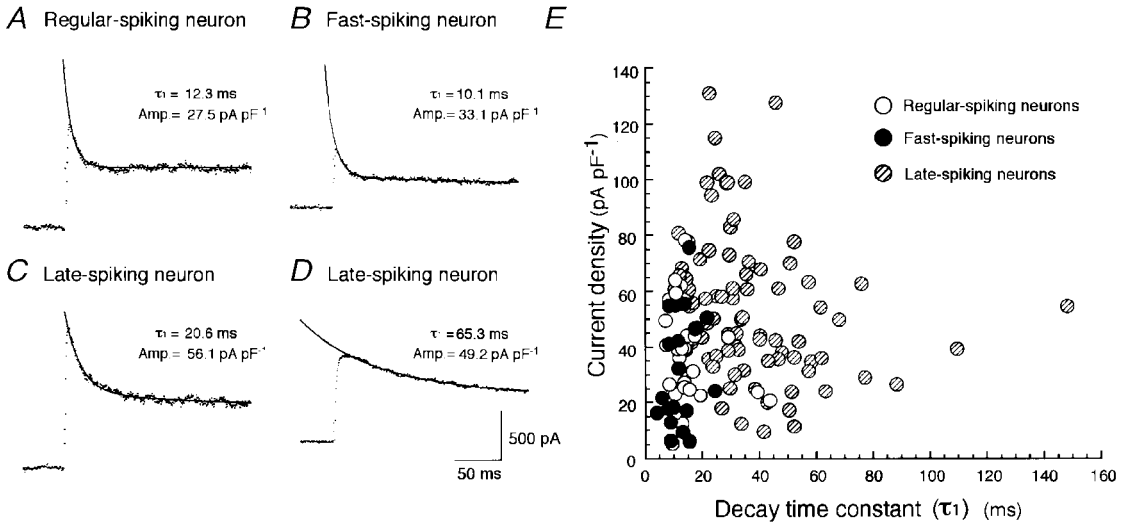

Figure 3. Inactivation kinetics and current density of TOCs in the three neuron types

A–D, TOCs (dotted traces) and double-exponential fits superimposed on the decay phase in regular-spiking (*A*), fast-spiking (*B*) and late-spiking neurons (*C* and *D*). *E*, relationship between the current density and the decay time constant (τ_1). ○, regular-spiking neurons; ●, fast-spiking neurons; ⊘, late-spiking neurons.

difference in the decay time constant and the current density between TOCs in regular-spiking neurons and those in fast-spiking neurons ($P > 0{\cdot}1$, t test). On the other hand, TOCs in late-spiking neurons ($n = 83$, ⊘ in Fig. 3*E*) exhibited a wide range of values for both inactivation kinetics ($36{\cdot}7 \pm 2{\cdot}4$ ms, with a range from 11·3 to 147·8 ms) and current density ($54{\cdot}0 \pm 2{\cdot}9$ pA pF^{-1}, with a range from 9·8 to 131·2 pA pF^{-1}). Figure 3*C* exemplifies a TOC exhibiting fast inactivation kinetics with a large current density, while Fig. 3*D* shows a TOC with slow inactivation kinetics. The current density of TOCs in late-spiking neurons with τ_1 values smaller than 30 ms ($62{\cdot}6 \pm 4{\cdot}3$ pA pF^{-1}, $n = 38$) was significantly larger than those in regular- and fast-spiking neurons ($P < 0{\cdot}0001$, ANOVA *post hoc* test).

The analysis of the inactivation kinetics of TOCs revealed that late-spiking neurons displayed TOCs with a wide range of decay time constants. Therefore, in subsequent experiments, in order to analyse TOCs with fast and slow decay time constants (τ_1) in late-spiking neurons separately, we limited our analysis to two extreme populations of late-spiking neurons and thereafter designated the neurons having TOCs with τ_1 faster than 30 ms as class I late-spiking neurons and those having TOCs with τ_1 slower than 50 ms as class II late-spiking neurons. Late-spiking neurons displaying TOCs with intermediate decay time constants (30 ms $< \tau_1 <$ 50 ms) were not analysed further in the present study.

Activation kinetics of TOCs

The activation kinetics of TOCs were defined as the time taken for the current to rise from 10 to 90% of its peak amplitude. The analysis was carried out on TOCs induced by a test pulse to −10 mV. The rise times of TOCs in regular-spiking ($n = 13$), fast-spiking ($n = 10$), class I late-spiking ($n = 24$) and class II late-spiking ($n = 7$) neurons were $2{\cdot}9 \pm 0{\cdot}3$, $1{\cdot}9 \pm 0{\cdot}2$, $3{\cdot}1 \pm 0{\cdot}3$ and $5{\cdot}3 \pm 0{\cdot}5$ ms, respectively. The rise times of TOCs in class II late-spiking neurons were significantly slower than other neuron types ($P < 0{\cdot}01$, ANOVA *post hoc* test).

Recovery from inactivation of TOCs

The time course of recovery from inactivation was investigated using a double-pulse protocol. In this experiment, we added 10–30 mM TEA to the control solution to enable us to discern the peak of the TOCs without using the subtraction protocol. First, a 1 s depolarizing pulse to −10 mV (the first pulse) was applied following a prepulse to −100 mV to inactivate TOCs. Then,

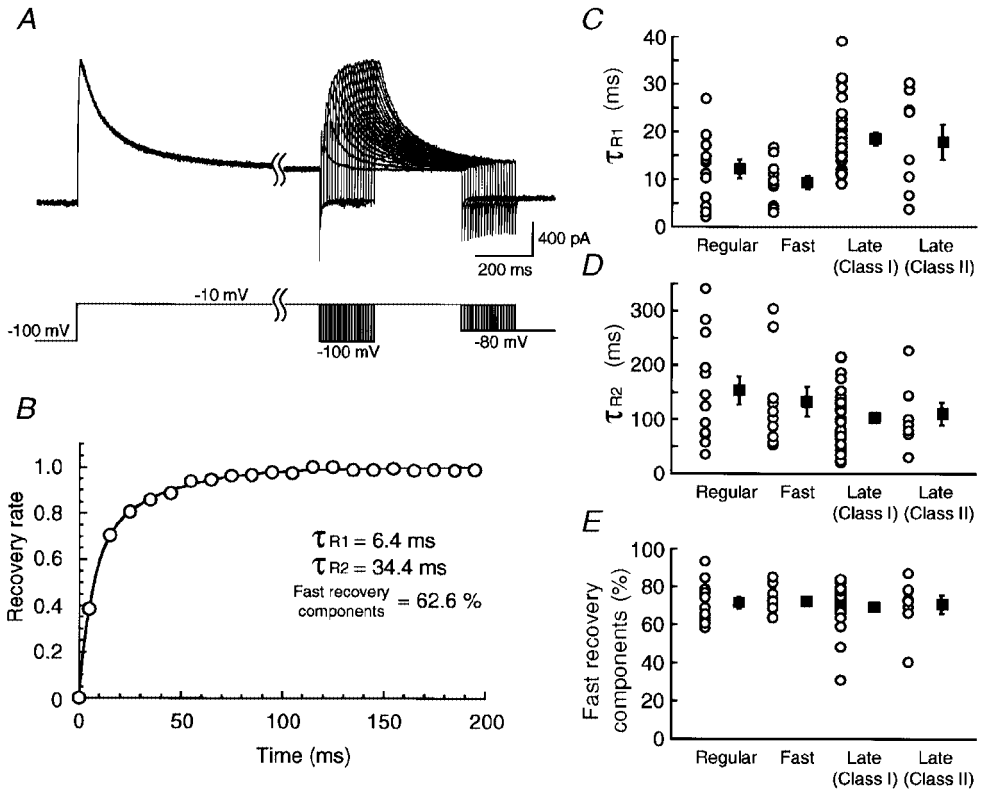

Figure 4. Recovery from inactivation of TOCs

A, an example of whole-cell outward currents evoked by the double-pulse protocol. *B*, time course of recovery from inactivation. *A* double-exponential fit is superimposed on the plots. *C–E*, fast recovery time constants (τ_{R1}), slow recovery time constants (τ_{R2}) and the percentage of fast recovery components in each neuron type, respectively. Plots of the time constants in individual neurons (○), the mean time constants (■) and S.E.M. (bars) are shown (*C–E*). Slow recovery time constants and the percentage of fast recovery components were not significantly different among the different neuron types ($P > 0{\cdot}1$, ANOVA *post hoc* test).

a prepulse to −100 mV for 5–195 ms in 10 ms increments followed by a 0·5 s test pulse to −10 mV (the second pulse) were applied (Fig. 4*A*). Plots of the recovery rates obtained from the peak currents evoked by the second pulse divided by those evoked by the first pulse as a function of prepulse duration were fitted with a sum of two exponential functions (Fig. 4*B*). Figure 4*C–E* shows plots of fast (τ_{R1}) and slow (τ_{R2}) recovery time constants, and the percentage of fast recovery components in regular-spiking ($n = 13$), fast-spiking ($n = 10$), class I late-spiking ($n = 28$) and class II late-spiking ($n = 8$) neurons. Fast recovery time constants in fast-spiking neurons were significantly different from those in class I late-spiking neurons ($P < 0{\cdot}01$, ANOVA *post hoc* test). In all neuron types, fast recovery components dominated (Fig. 4*E*) and were not different among the neuron types ($P > 0{\cdot}1$, ANOVA *post hoc* test).

Voltage dependence of activation, steady-state inactivation and decay time constant of TOCs

The voltage dependence of activation, steady-state inactivation and decay time constant of TOCs was analysed in a total of seven regular-spiking, seven fast-spiking, six class I late-spiking, and four class II late-spiking neurons (Fig. 5). The mean values of normalized chord conductance, obtained from the amplitude of the fast-inactivating component (A_1) of TOCs isolated with the subtraction protocol described above, were plotted as a function of the test pulse potential (Fig. 5*A1–D1*, ●). These plots were fitted with the Boltzmann function:

$$G(V_m)/G_{max} = 1/\{1 + \exp[-(V_m - V_{½})/k]\},$$

where $G(V_m)$ is the chord conductance at membrane potential V_m, G_{max} is maximal chord conductance, $V_{½}$ is the voltage of half-maximal conductance, and k is a slope factor. Comparison of the voltage of half-maximal conductance and the slope factor among the four neuron types (Fig. 5*A1–D1*, see tables below graphs) revealed that TOCs in class II late-spiking neurons were activated at the most hyperpolarized membrane potential ($V_{½} = -41{\cdot}7$ mV). On the other hand, TOCs in fast-spiking neurons showed a high threshold of activation ($V_{½} = -24{\cdot}9$ mV).

The voltage dependence of steady-state inactivation was studied by applying 1 s depolarizing voltage steps to −10 mV following a series of 500 ms prepulses between −120 and −20 mV at 10 mV intervals. The normalized

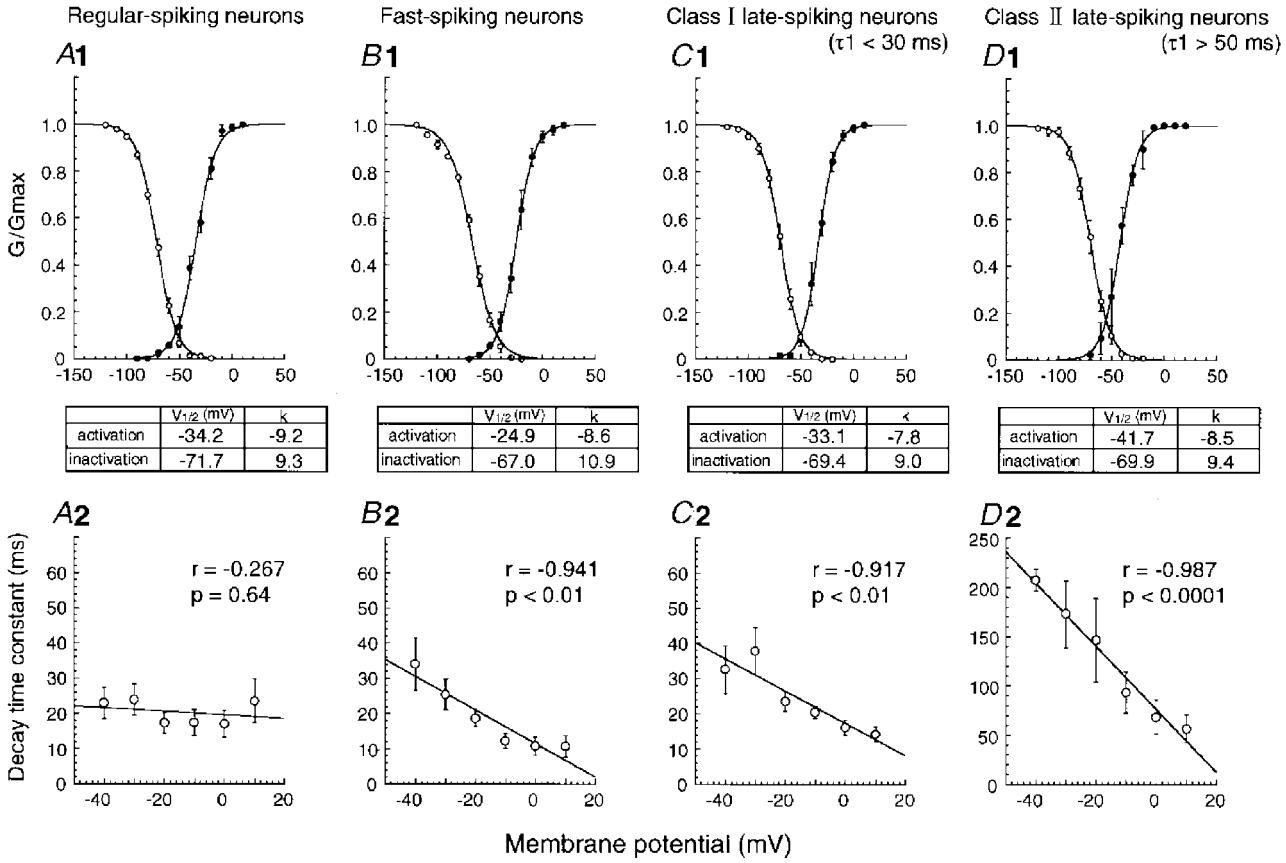

Figure 5. Voltage dependence of activation, steady-state inactivation and decay time constant of TOCs

A1–D1, plots of the mean normalized chord conductances as a function of the membrane potentials in regular-spiking, fast-spiking, class I late-spiking and class II late-spiking neurons, respectively. Boltzman fits are superimposed on the plots of activation (●) and inactivation (○) with bars indicating S.E.M. A voltage of half-maximal conductance and a slope factor are shown in the tables between the panels. *A2–D2*, plots of decay time constants as a function of test pulse potentials.

chord conductance was calculated from the peak amplitude of the total outward current, and plotted as a function of the prepulse potential (Fig. 5*A*1–*D*1, ○). These plots were also fitted with a Boltzmann function:

$$G(V_m)/G_{max} = 1/\{1 + \exp[(V_m - V_{½})/k]\}.$$

There was no apparent difference in the voltage dependence of steady-state inactivation among the neuron types.

In the present study, 0·2 mM Cd^{2+} was added to the control solution to block the Ca^{2+} current (see Methods). Previous studies suggest that divalent cations alter the voltage dependence of activation and steady-state inactivation of A-type currents (Mayer & Sugiyama, 1988; Andreasen & Hablits, 1992; Song *et al.* 1998). Although we did not investigate the effect of Cd^{2+} on the voltage dependence, Andreasen & Hablits (1992) reported that the presence of extracellular 0·2 mM Cd^{2+} caused a shift in the voltage of half-activation of approximately +20 mV, suggesting that the values of the voltage of half-activation obtained in the present study were approximately 20 mV more positive than those in the absence of Cd^{2+}. Therefore, TOCs in fast-spiking neurons may be involved in determining firing patterns at above or near the threshold level for spike generation (about −48 mV, see above), and TOCs in other types of neurons at subthreshold levels (see above).

The voltage dependence of the fast decay time constant (τ_1) is shown in Fig. 5*A*2–*D*2. The analysis was performed using the same neurons as in *A*1–*D*1. Plots of τ_1 against test pulse potentials revealed that τ_1 was independent of voltage in regular-spiking neurons and was dependent on voltage in

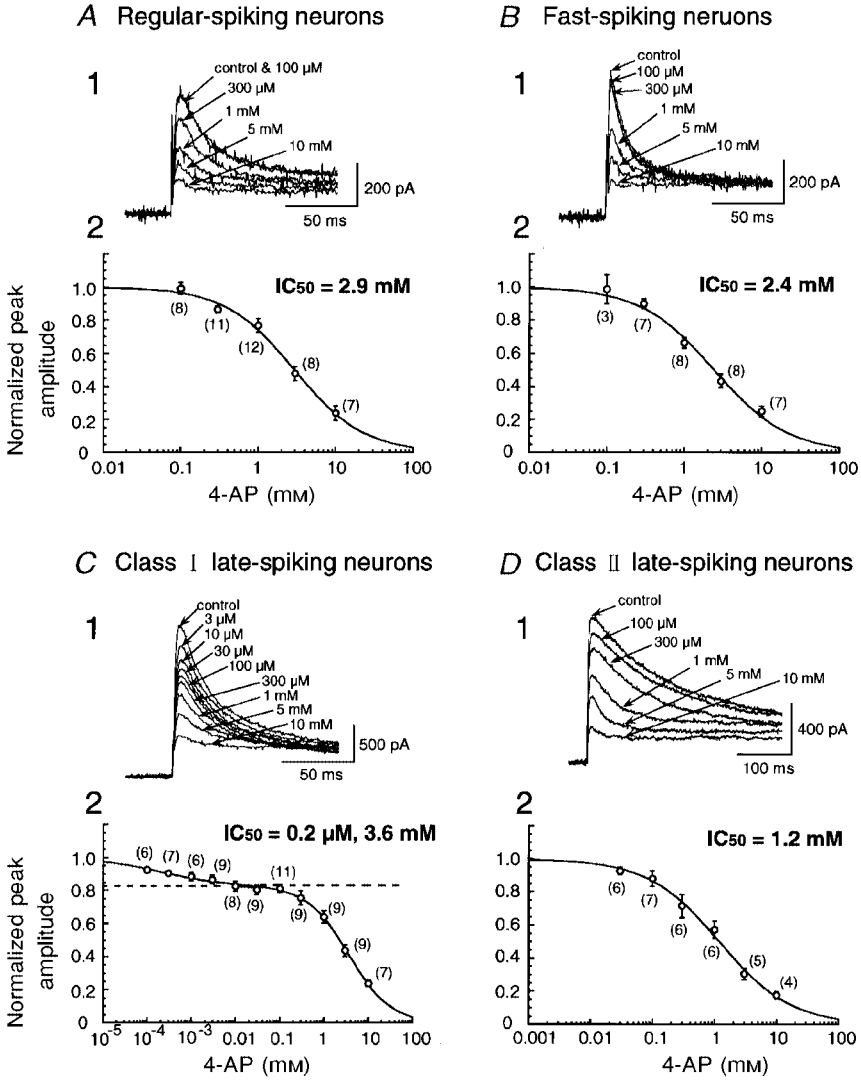

Figure 6. Sensitivity to 4-AP of TOCs

*A*1–*D*1, recordings of TOCs in the presence of different concentrations of 4-AP in regular-spiking, fast-spiking, class I late-spiking and class II late-spiking neurons, respectively. *A*2–*D*2, dose–response curves for 4-AP. The numbers in parentheses indicate the number of neurons tested. Note that the plots of the normalized peak amplitude of TOCs in class I late-spiking neurons against the concentration of 4-AP were fitted by the sum of two logistic functions (*C*2).

fast- and late-spiking neurons. In class II late-spiking neurons, τ_1 was strongly dependent on test pulse potentials.

Sensitivity to 4-aminopyridine

It has been shown that TOCs are suppressed by 4-aminopyridine (4-AP) (Gustafsson *et al.* 1982; Thompson, 1982). To investigate the pharmacological properties of TOCs in neurons with different firing properties, dose–response curves of inhibition by 4-AP were obtained from a total of 17 regular-spiking, 8 fast-spiking, 28 class I late-spiking, and 10 class II late-spiking neurons. We replaced NMG in the control solution with 25 mM TEA, because stable recordings of TOCs were obtained for a long period in the presence of TEA. Since TEA at this concentration did not suppress sustained outward currents completely, TOCs were isolated by applying the subtraction protocol described above (Fig. 2). Application of 4-AP reduced the peak amplitude of TOCs in a dose-dependent manner (Fig. 6*A*1–*D*1). Plots of the normalized amplitude of TOCs against the concentration of 4-AP in regular-spiking, fast-spiking and class II late-spiking neurons were fitted by the single logistic function:

$$I/I_{\mathrm{cont}} = 1/\{1 + ([\text{4-AP}]_{\mathrm{o}}/m)^n\},$$

where I_{cont} is the amplitude of current in the control solution, $[\text{4-AP}]_{\mathrm{o}}$ is the concentration of 4-AP in the bath solution, m is the value of IC_{50}, and n is the Hill coefficient (Fig. 6*A*2, *B*2 and *D*2). The values of IC_{50} in regular-spiking, fast-spiking and class II late-spiking neurons were 2·9, 2·4 and 1·2 mM, respectively. The Hill coefficient in regular- and fast-spiking neurons was nearly 1·0. On the other hand, the Hill coefficient in class II late-spiking neurons was smaller than 1·0 ($n = 0{\cdot}75$), suggesting negative co-operativity or multiple apparent sites of action. In contrast, the plots in class I late-spiking neurons were well fitted by the sum of two logistic functions (Fig. 6*C*2):

$$I/I_{\mathrm{cont}} = a/\{1 + ([\text{4-AP}]_{\mathrm{o}}/m_1)^{n_1}\} + (1 - a)/\{1 + ([\text{4-AP}]_{\mathrm{o}}/m_2)^{n_2}\} \quad (0 < a < 1),$$

where a is the normalized peak amplitude and m_2 is larger than m_1. The values of m_1 and m_2 were 0·2 μM and 3·6 mM, respectively. The value of n_1 was smaller than 1·0 ($n_1 = 0{\cdot}60$), although that of n_2 was nearly 1·0. This result suggests that TOCs with fast inactivation kinetics are composed of at least two components, although the component highly sensitive to 4-AP is not large in amplitude ($a = 0{\cdot}17$; see Fig. 6*C*2). The decay time constant of the component highly sensitive to 4-AP, which was estimated from the component blocked by 100 μM 4-AP, was 19·4 ± 0·5 ms ($n = 18$).

Effect of 4-aminopyridine on late-spiking properties

Since the sensitivity to 4-AP differed among late-spiking neurons according to the difference in inactivation kinetics (Fig. 6), we investigated the effect of 4-AP on the firing property of late-spiking neurons. In current clamp mode, class I late-spiking neurons exhibited short 1st ISIs (75·0 ± 7·7 ms, with a range from 19·0 to 257·4 ms, $n = 38$). In contrast, class II late-spiking neurons exhibited long 1st ISIs (176·6 ± 18·8 ms, with a range from 72·2 to 369·0 ms, $n = 19$). Therefore, we compared the effect of 4-AP on neurons with a 1st ISI shorter than 50 ms, presumably class I late-spiking neurons, with those with a 1st ISI longer than 150 ms, presumably class II late-spiking neurons. The late-spiking property was estimated according to whether the ratio of the 1st ISI to the 2nd ISI was larger than 1·0 or not (see Fig. 1*D*). Low concentrations of 4-AP (50 μM) changed the firing pattern of the late-spiking neurons with the short 1st ISI to the regular-spiking mode (Fig. 7*A*1 and 2). It can be noted that the fast after-hyperpolarization of each action potential was diminished (the second sweep in Fig. 7*A*1). In four of five late-spiking neurons with a short 1st ISI, application of 10 μM 4-AP was also effective in eliminating the late-spiking property (Fig. 7*D*). In contrast, the neurons with a long 1st ISI still exhibited late spiking, and the amplitude of fast after-hyperpolarization remained virtually unchanged in the presence of 50 μM 4-AP (the second sweep in Fig. 7*B*1). The late-spiking property of late-spiking neurons with a long 1st ISI remained in the presence of 100 μM 4-AP, although the 1st ISI and the ratio of the 1st ISI to the 2nd ISI became smaller (Fig. 7, the third sweep in *B*1, and *B*2). In the presence of high concentrations of 4-AP (5 mM, Fig. 7*B*1 and 2), they changed to regular spiking and the fast after-hyperpolarization disappeared. Figure 7*C* shows the mean ratio of the 1st ISI to the 2nd ISI plotted against the concentration of 4-AP in late-spiking neurons with the short (■) and long 1st ISIs (□).

The effects of low concentrations of 4-AP (10 or 50 μM application for < 1 min) on the late-spiking neurons with a short 1st ISI could be reversed more than 7 min after washing out 4-AP (see Fig. 7*D*), but the effects of high concentrations of 4-AP could only be partially reversed or were irreversible.

Contribution of non-inactivating outward currents to late-spiking neurons

In late-spiking neurons, application of 4-AP decreased the amplitude of TOCs (Fig. 6*C* and *D*) and changed the firing patterns to the regular-spiking mode (Fig. 7), suggesting that TOCs contribute to the late-spiking property. In particular, low concentrations (< 50 μM) of 4-AP eliminated the firing patterns of late-spiking neurons with a short 1st ISI (Fig. 7*A*, *C* and *D*), suggesting that the components of TOCs with high sensitivity to 4-AP (Fig. 6*C*) contribute to the late-spiking property. Late-spiking properties have been thought to be caused by 4-AP-sensitive, slowly or non-inactivating potassium currents (e.g. D-type currents) as well as TOCs (Storm, 1988; Wu & Barish, 1992; Foehring & Surmeier, 1993; Lüthi *et al.* 1996). Therefore, to investigate the possibility of a contribution of 4-AP-sensitive non-inactivating outward currents to the late-spiking property, we analysed the effects of 4-AP on the outward currents induced by a test pulse to −10 mV from a prepulse to −30 mV (Fig. 8). Since we obtained non-inactivating

currents in the presence of 25 mM TEA, a major component of the currents may be D-type currents, although the concentration of TEA used may have been insufficient to block delayed K^+ channels completely. The current amplitude of non-inactivating outward currents was estimated from the mean amplitude between 900 and 950 ms after the onset of the test pulse. In class I late-spiking neurons (Fig. 8*A*), application of 30 μM 4-AP decreased the amplitude of non-inactivating outward currents (by 21·9 ± 0·03 % of the control value, $n = 4$). However, the amplitude of the currents did not show any obvious decrease after application of higher concentrations of 4-AP (currents decreased by 28·5 ± 0·03 % of the control value with 100 μM). These results suggest that non-inactivating outward currents as well as TOCs were sensitive to low concentrations of 4-AP which changed the firing pattern of class I late-spiking neurons to the regular-spiking mode. To investigate further the contribution of non-inactivating outward currents to the late-spiking property, we analysed the effect of dendrotoxin, which is a selective blocker of Kv1.1, 1.2 and 1.6 channels (Stühmer *et al.* 1989; Pongs, 1992), on class I late-spiking neurons. In current-clamp recordings, late-spiking neurons with a short 1st ISI changed their firing patterns to the regular-spiking mode following application of 200 nM dendrotoxin ($n = 4$, Fig. 9*A* and *B*), suggesting the contribution of non-inactivating outward currents to the late-spiking property. However, voltage-clamp recordings revealed that both inactivating and non-inactivating outward currents were sensitive to dendrotoxin (Fig. 9*C*). The mean current densities of dendrotoxin-sensitive inactivating currents, obtained from the peak amplitude, and of dendrotoxin-sensitive non-inactivating currents, obtained from the mean amplitude between 900 and 950 ms after the onset of the test pulse, were 13·3 ± 3·2 and 3·4 ± 0·5 pA pF^{-1} ($n = 6$), respectively. Since dendrotoxin affected both inactivating and non-inactivating currents, which may correspond to the components of TOCs with a high sensitivity to 4-AP and 4-AP-sensitive non-inactivating outward currents, respectively, it remains an open question which of them

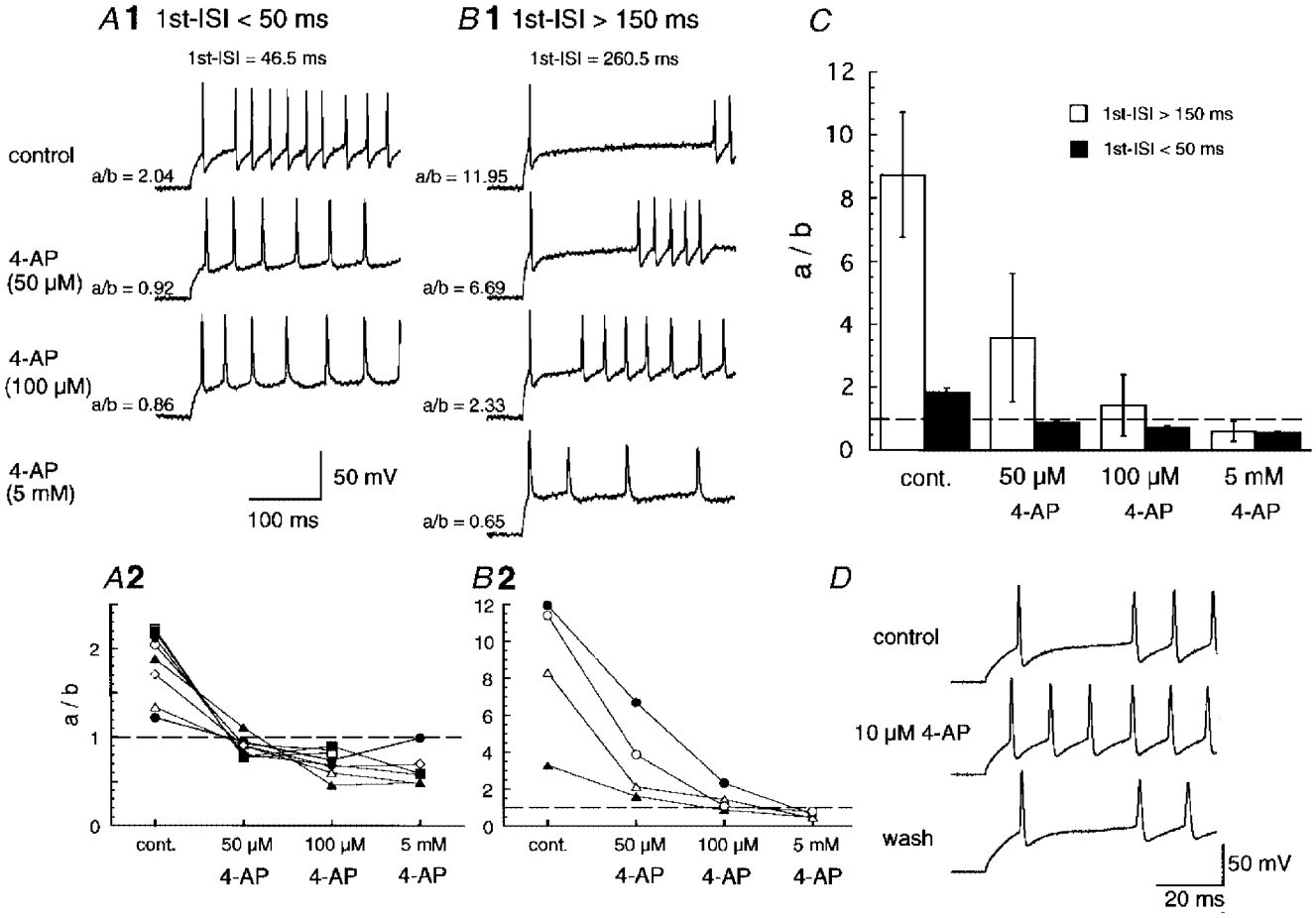

Figure 7. Effect of 4-AP on firing patterns of late-spiking neurons

*A*1 and *B*1, effect of 4-AP on late-spiking neurons with the 1st ISI shorter than 50 ms (40·2 ± 4·4 ms, $n = 8$) and longer than 150 ms (182·8 ± 26·0 ms, $n = 4$), respectively. *A*2 and *B*2, plots of the ratio of the 1st ISI to the 2nd ISI (a/b) as a function of concentration of 4-AP. Individual symbols represent the plots obtained from individual neurons. Dashed lines indicate a ratio value of 1·0. *C*, the mean ratio of the 1st ISI to the 2nd ISI (a/b) against the concentration of 4-AP in late-spiking neurons with a 1st ISI < 50 ms (■) and > 150 ms (□). *D*, effect of 10 μM 4-AP on late-spiking neurons with the 1st ISI < 50 ms. The late-spiking property was recovered 10 min after washing out 4-AP.

contributes to the late-spiking property in class I late-spiking neurons.

In class II late-spiking neurons (Fig. 8*B*), the amplitude of non-inactivating outward currents also decreased after application of 100 μM 4-AP (by 17·7 $\pm$ 0·1 % of the control value, $n = 4$). However, no further decrease in the amplitude of the currents was seen with 3 mM 4-AP (the current decreased by 10·7 $\pm$ 0·1 % of the control value). In contrast, TOCs were decreased markedly after application of 3 mM 4-AP (Fig. 8*B*4). These results suggest that the non-inactivating outward currents were not sensitive to the high concentrations of 4-AP which changed the firing pattern of class II late-spiking neurons to the regular-spiking mode. Application of 200 nM dendrotoxin to late-spiking neurons with a long 1st ISI decreased the 1st ISI and the ratio of the 1st ISI to the 2nd ISI, but did not affect the late-spiking property (Fig. 9*D* and *E*). Taken together, the results suggest that TOCs contribute to the late-spiking property in class II late-spiking neurons.

DISCUSSION

In the present study, we found that TOCs in the three neuron types showed different electrophysiological and pharmacological properties. In regular-spiking neurons, TOCs showed fast inactivation kinetics, a small current density and activation at membrane potentials below the threshold for generation of action potentials. In fast-spiking neurons, TOCs showed fast inactivation kinetics, a small current density, relatively fast activation kinetics, and activation at membrane potential above the threshold for generation of action potentials. In class I late-spiking neurons, TOCs showed fast inactivation kinetics, a large current density, and the existence of a component highly sensitive to 4-AP. In class II late-spiking neurons, TOCs showed slow inactivation kinetics and activation at the most hyperpolarized membrane potential. These different properties of TOCs, therefore, may determine the different firing patterns.

Different properties of TOCs among neurons with different firing patterns

The present study has shown that TOCs in neurons with different firing patterns exhibit different electrophysiological properties. Previous studies have described TOCs with different electrophysiological properties in neurons of other regions in the CNS. Voltage-clamp studies of cultured neostriatal neurons showed that the neurons exhibited two types of TOCs with different voltage dependence of activation (Surmeier *et al.* 1989). In the rat piriform cortex, TOCs in neurons in the endopiriform nucleus (EN) and those in layer II (LII) pyramidal neurons exhibited different properties; TOCs in LII pyramidal neurons showed a larger amplitude and faster activation and inactivation kinetics than those in EN neurons (Banks *et al.*

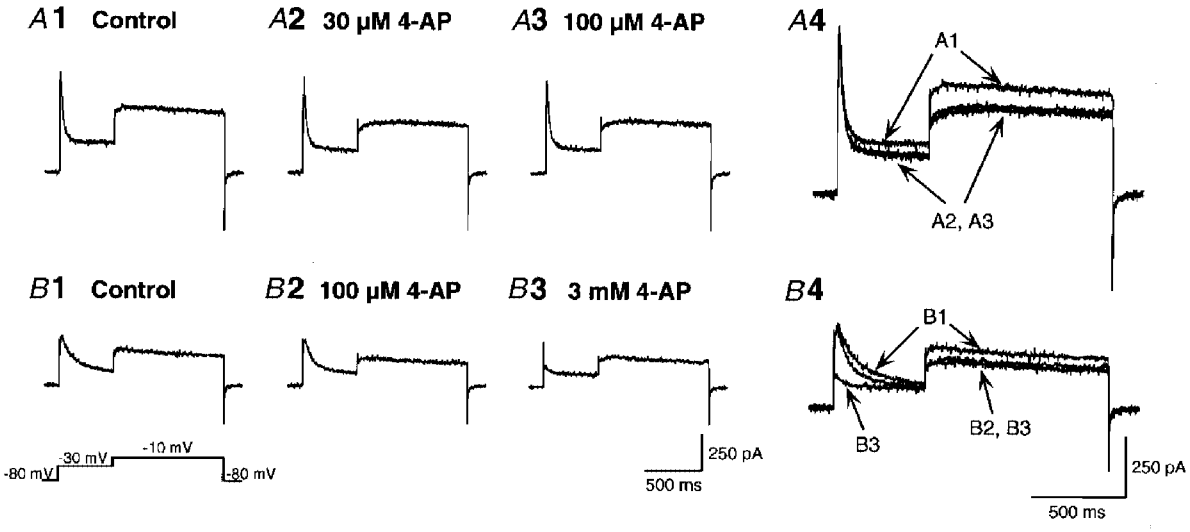

Figure 8. Effect of 4-AP on non-inactivating outward currents

Outward currents evoked by a test pulse to −10 mV following a prepulse to −30 mV. Non-inactivating outward currents are represented as outward currents evoked by a test pulse. *A*, non-inactivating outward currents in class I late-spiking neurons in the control solution (1), and in the presence of 30 μM (2) and 100 μM (3) 4-AP. *A*4 shows the three traces of *A*1–3 superimposed. Note that the non-inactivating outward current was decreased following application of 30 μM 4-AP, but no further decrease was seen with 100 μM 4-AP. *B*, non-inactivating outward currents in class II late-spiking neurons in control solution (1), and in the presence of 100 μM (2) and 3 mM (3) 4-AP. *B*4 shows the three traces of *B*1–3 superimposed. Note that the non-inactivating outward current was decreased following application of 100 μM 4-AP, but no further decrease was seen with 3 mM 4-AP. An inactivating outward current, which was evoked by a prepulse, was mostly abolished by application of 3 mM 4-AP. The voltage protocol is shown at bottom left.

1996). Neurons in the lateral (LOC) and medial olivocochlear (MOC) nuclei also exhibited TOCs with different activation and inactivation kinetics and recovery times from inactivation (Fujino *et al.* 1997). The authors proposed that the different properties might be responsible for the different firing patterns of LOC and MOC neurons.

These different properties of TOCs might be explained simply by differences among cells in the distribution of TOC channels on the soma–dendritic membrane. However, simulation studies on the degree of attenuation of TOCs with a particular electrotonic distance from the soma indicated that some of the different properties of TOCs were caused by intrinsic channel properties rather than different distributions of TOC channels (Banks *et al.* 1996). In the present study, the sensitivity of TOCs to 4-AP appeared not to be identical in the different neuron types (Figs 5 and 6), suggesting that the channel properties are different.

If the different properties of TOCs are caused by differences in the intrinsic channel properties, a difference between neurons in the expression pattern of the Kv α-subunits comprising the A-type channels can be considered. *In situ* hybridization analysis revealed that among α-subunits giving rise to A-type currents (Kv1.4, 3.4, 4.1, 4.2 and 4.3), the Kv3.4 subunit showed patchy expression in the SGI of the SC (Weiser *et al.* 1994). Kv4.2 and Kv4.3 subunits were also expressed in the SC, although the Kv4.3 subunit was mainly expressed in the deep region of the superficial layer (the stratum opticum) (Serôdio *et al.* 1996; Tsaur *et al.* 1997). From our analysis of the voltage dependence of the inactivation time constant in the present study, we suggest that TOCs in regular-spiking neurons are dominated by Kv4 subunits and those in the other neuron types are dominated by Kv1.4 subunits (Tseng-Crank *et al.* 1990; Serôdio *et al.* 1994). However, we did not observe a difference in the time course of recovery from inactivation sufficient to support the difference in the constituting subunits (see Ruppersberg *et al.* 1990). Some portion of TOCs in class I late-spiking neurons were sensitive to dendrotoxin (Fig. 9*C*), suggesting the involvement of Kv1.1, 1.2, or 1.6 subunits

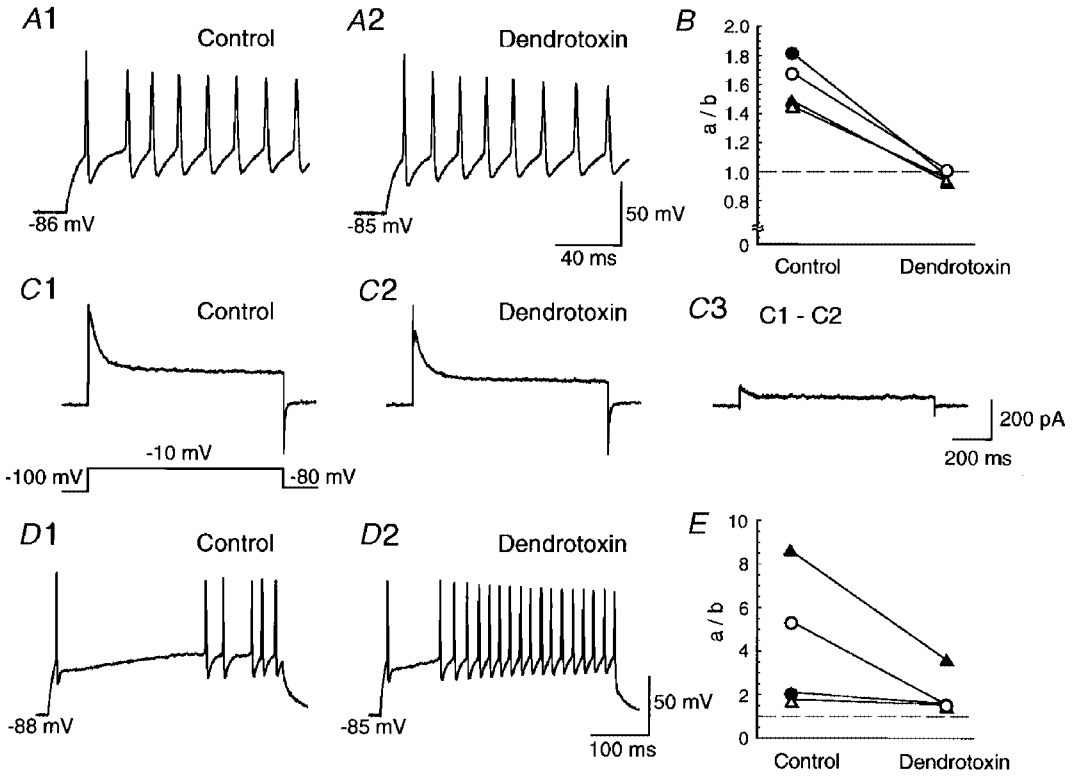

Figure 9. Effect of dendrotoxin on late-spiking neurons

A, firing pattern of a late-spiking neuron with a short 1st ISI (31·1 ± 5·2 ms, $n = 4$) in control solution (1) and in the presence of 200 nM dendrotoxin (2). *B*, plots of the ratio of the 1st ISI to the 2nd ISI in the absence and presence of dendrotoxin. Individual symbols represent the plots obtained from individual neurons. The dashed line indicates the ratio value of 1·0. *C*, whole-cell outward currents in control solution (1) and in the presence of 200 nM dendrotoxin (2) in a class I late-spiking neuron. *C*3 shows a dendrotoxin-sensitive current obtained by subtraction of *C*2 from *C*1. Note that both inactivating and non-inactivating currents are sensitive to dendrotoxin. *D*, firing pattern in a late-spiking neuron with a long ISI (212·9 ± 24·2 ms, $n = 4$) in control solution (1) and in the presence of 200 nM dendrotoxin (2). *E*, plots of the ratio of the 1st ISI to the 2nd ISI in the absence and presence of dendrotoxin.

(Stühmer *et al.* 1989; Pongs, 1992). All these data suggest that the difference in the expression pattern of the α-subunits is not the only factor involved in the different properties of TOCs, and some other factors such as the modulation of channels, for example a contribution from β-subunits, which have been shown to be expressed in the SC (Rhodes *et al.* 1996; Butler *et al.* 1998), and phosphorylation by several protein kinases (reviewed in Jonas & Kaczmarek, 1996) may be involved.

It has also been shown that the expression of A-type currents varies during development (Costa *et al.* 1994; Klee *et al.* 1995). In rats aged 17–22 days, which were used in the present study because of their accessibility, the SC may still be in the course of development (e.g. Warton & Jones, 1985), suggesting that TOCs have not completed their maturation. However, in our previous study we identified the three firing patterns of the SGI neurons investigated in the present study in rats aged 7–8 weeks (Saito & Isa, 1999). Furthermore, late-spiking neurons with a 1st ISI longer than 150 ms, as well as those with a 1st ISI shorter than 50 ms, could be observed in adult rats (Y. Saito & T. Isa unpublished observation). Although we did not investigate the properties of TOCs in the SGI neurons in adult rats, the fact that the different firing patterns can be observed even in adult rats suggests that the different properties of TOCs among different neuron types in young rats do not simply reflect the difference in their maturation level.

Putative contribution of TOCs to the difference in firing patterns

From our analysis of the voltage dependence of activation, it appears that TOCs in regular-spiking neurons may be activated at a membrane potential below the threshold for spike generation, suggesting that they regulate generation of action potentials. The properties of activation at the subthreshold level and the fast inactivation of the TOCs may control interspike intervals (Connor & Stevens, 1971), and thus make the firing pattern of regular-spiking neurons relatively constant. On the other hand, TOCs in fast-spiking neurons may be mostly activated near or above the threshold for spike generation, suggesting that they regulate the width of individual action potentials. This is supported by the relatively constant spike width during a spike train (Fig. 1*E*). The fast activation kinetics of the TOCs may not only make it possible to sharpen individual action potentials but may also help to remove inactivation of sodium channels. Furthermore, in fast-spiking neurons TOCs with a fast time constant for recovery from inactivation (< 10 ms; see Fig. 4*C*) exist, suggesting that some portion of TOCs can recover during high repetitive firings. Thus, TOCs in fast-spiking neurons enable the neurons to sustain high-frequency repetitive firing patterns. Other ionic conductances may also contribute to the fast-spiking properties. For example, the different gating properties of sodium channels contribute to the action potential patterns of hippocampal interneurons and principal neurons (Martina & Jonas, 1997). Non-inactivating potassium currents with fast activation kinetics, presumably arising from Kv3.1 subunits, are also considered to contribute to fast spiking (Perney & Kaczmarek, 1997; Wang *et al.* 1998). However, we did not examine the non-inactivating current in fast-spiking neurons in these experiments, and therefore it is not clear at present whether the non-inactivating currents exist and contribute to fast spiking in SGI neurons. In late-spiking neurons, the properties of TOCs are different among neurons with different 1st ISIs. TOCs in class I late-spiking neurons are activated at hyperpolarized membrane potentials and show fast activation and inactivation kinetics. These properties resemble those of TOCs in regular-spiking neurons. However, TOCs in class I late-spiking neurons were larger in amplitude than those in regular-spiking neurons (Fig. 3*E*) and included a component highly sensitive to 4-AP (Fig. 6). The change from late spiking to regular spiking following application of a low concentration of 4-AP (Fig. 7) suggests that components of TOCs which are highly sensitive to 4-AP contribute to the late-spiking property in class I late-spiking neurons. Non-inactivating outward currents sensitive to low concentrations of 4-AP were, however, present in class I late-spiking neurons (Fig. 8*A*), suggesting their contribution to the late-spiking property. Since both inactivating and non-inactivating currents were suppressed by application of dendrotoxin (Fig. 9*C*), we could not determine which of them contributed to the class I late-spiking property. To explore this issue further, a novel specific blocker or protocol to separate the two currents is needed. In any case, the late-spiking property in class I late-spiking neurons may be influenced by both TOCs highly sensitive to 4-AP and non-inactivating currents or by either of them. In class II late-spiking neurons, the slow inactivation of TOCs may cause the long interspike interval between the first and the second spikes. Although the activation kinetics of TOCs is slow in class II late-spiking neurons, a low threshold of activation prevents the neurons from firing immediately after the onset of the current pulse injection, giving them the late-spiking property. The non-inactivating currents sensitive to low concentrations of 4-AP were also present in class II late-spiking neurons (Fig. 8*B*). Application of high concentrations of 4-AP decreased or abolished TOCs, but did not further affect the non-inactivating currents. Class II late-spiking neurons shortened the 1st ISI in response to low concentrations of 4-AP and changed their firing patterns to the regular-spiking mode in response to high concentrations of 4-AP, suggesting that TOCs contribute to the late-spiking property, and non-inactivating currents lengthen the 1st ISI. Application of dendrotoxin did not completely abolish the late-spiking property, but decreased the 1st ISI (Fig. 9*D* and *E*), supporting this idea. Thus, pharmacological experiments that take advantage of the difference in sensitivity of TOCs to 4-AP and dendrotoxin could reveal the role of particular conductances in determining the firing patterns of the neurons.

Andreasen, M. & Hablitz, J. J. (1992). Kinetic properties of a transient outward current in rat neocortical neurons. *Journal of Neurophysiology* **68**, 1133–1142.

Banks, M. I., Haberly, L. B. & Jackson, M. B. (1996). Layer-specific properties of the transient K current (I_A) in piriform cortex. *Journal of Neuroscience* **16**, 3862–3876.

Baxter, D. A. & Byrne J. H. (1991). Ionic conductance mechanisms contributing to the electrophysiological properties of neurons. *Current Opinion in Neurobiology* **1**, 105–112.

Butler, D. M., Ono, J. K., Chang, T., McCaman, R. E. & Barish, M. E. (1998). Mouse brain potassium channel beta1 subunit mRNA: cloning and distribution during development. *Journal of Neurobiology* **34**, 135–150.

Chandy, K. G. & Gutman, G. A. (1995). Voltage-gated K^+ channel genes. In *Handbook of Receptors and Channels: Ligand- and Voltage-gated Ion Channels*, ed. North, R. A., pp. 1–79. CRC Press, Boca Ralton, FL, USA.

Connor, J. A. & Stevens, C. F. (1971). Voltage clamp studies of a transient outward membrane current in sagtropod neural somata. *Journal of Physiology* **213**, 21–30.

Connors, B. W. & Gutnick, M. J. (1990). Intrinsic firing patterns of diverse neocortical neurons. *Trends in Neurosciences* **13**, 99–103.

Costa, P. F., Santos, A. I. & Ribeiro, M. A. (1994). Potassium currents in acutely isolated maturing rat hippocampal CA1 neurones. *Developmental Brain Research* **83**, 216–223.

Dekin, M. S., Getting, P. A. & Johnson, S. M. (1987). *In vitro* characterization of neurons in the ventral part of the nucleus tractus solitarius. I. Identification of neuronal types and repetitive firing properties. *Journal of Neurophysiology* **58**, 195–214.

Dolly, J. O. & Parcej, D. N. (1996). Molecular properties of voltage-gated K^+ channels. *Journal of Bioenergetics and Biomembranes* **28**, 231–253.

Ficker, E. & Heinemann, U. (1992). Slow and fast transient potassium currents in cultured rat hippocampal cells. *Journal of Physiology* **445**, 431–455.

Foehring, R. C. & Surmeier, D. J. (1993). Voltage-gated potassium currents in acutely dissociated rat cortical neurons. *Journal of Neurophysiology* **70**, 51–63.

Fujino, K., Koyano, K. & Ohmori, H. (1997). Lateral and medial olivocochlear neurons have distinct electrophysiological properties in the rat brain slice. *Journal of Neurophysiology* **77**, 2788–2804.

Gean, P.-W. & Shinnick-Gallagher, P. (1989). The transient potassium current, the A-current, is involved in spike frequency adaptation in rat amygdala neurons. *Brain Research* **480**, 160–169.

Gustafsson, B., Galvan, M., Grafe, P. & Wigstrom, H. (1982). A transient outward current in a mammalian central neurone blocked by 4-aminopyridine. *Nature* **299**, 252–254.

Han, Z.-S., Buhl, E. H., Lörinczi, Z. & Somogyi, P. (1993). A high degree of spatial selectivity in the axonal and dendritic domains of physiologically identified local circuit neurons in the dentate gyrus of the rat hippocampus. *European Journal of Neuroscience* **5**, 395–410.

Hille, B. (1992). *Ionic Channels of Excitable Membranes.* Sinauer, Sunderland, MA, USA.

Isa, T., Endo, T &. Saito, Y. (1998). The visuo-motor pathway in the local circuit of the rat superior colliculus. *Journal of Neuroscience* **18**, 8496–8504.

Jonas, E. A. & Kaczmarek, L. K. (1996). Regulation of potassium channels by protein kinases. *Current Opinion in Neurobiology* **6**, 318–323.

Kang, Y. & Kitai, S. T. (1990). Electrophysiological properties of pedunculopontine neurons and their postsynaptic responses following stimulation of substantia nigra reticulata. *Brain Research* **535**, 79–95.

Kawaguchi, Y. (1995). Physiological subgroups of nonpyramidal cells with specific morphological characteristics in layer II/III of rat frontal cortex. *Journal of Neuroscience* **15**, 2638–2655.

Klee, R., Ficker, E. & Heinemann, U. (1995). Comparison of voltage-dependent potassium currents in rat pyramidal neurons acutely isolated from hippocampal regions CA1 and CA3. *Journal of Neurophysiology* **74**, 1982–1995.

Llinás, R. (1988). The intrinsic electrophysiological properties of mammalian neurons: Insights into central nervous system function. *Science* **242**, 1654–1664.

Lüthi, A., Gähwiler B. H. & Gerber U. (1996). A slowly inactivating potassium current in CA3 pyramidal cells of rat hippocampus *in vitro*. *Journal of Neuroscience* **16**, 586–594.

McCormick, D. A., Conners, B. W., Lighthall, J. W. & Prince, D. A. (1985). Comparative electrophysiology of pyramidal and sparsely spiny stellate neurons of the cortex. *Journal of Neurophysiology* **54**, 782–806.

Martina, M. & Jonas, P. (1997). Functional differences in Na^+ channel gating between fast-spiking interneurones and principal neurones of rat hippocampus. *Journal of Physiology* **505**, 593–603.

Mayer, M. L. & Sugiyama, K. (1988). A modulatory action of divalent cations on transient outward current in cultured rat sensory neurones. *Journal of Physiology* **396**, 417–433.

Perney, T. M. & Kaczmarek, L. K. (1997). Localization of a high threshold potassium channel in the rat cochlear nucleus. *Journal of Comparative Neurology* **386**, 178–202.

Pongs, O. (1992). Molecular biology of voltage-dependent potassium channels. *Physiological Reviews* **72**, S69–88.

Rhodes, K. J., Monaghan, M. M., Barrezueta, N. X., Nawoschik, S., Bekele-Arcuri, Z., Matos, M. F., Nakahira, K., Schechter, L. E. & Trimmer, J. S. (1996). Voltage-gated K^+ channel beta subunits: expression and distribution of Kv beta 1 and Kv beta 2 in adult rat brain. *Journal of Neuroscience* **16**, 4846–4860.

Rogawski, M. A. (1985). The A current: how ubiquitous a feature of excitable cells is it? *Trends in Neurosciences* **8**, 214–219.

Rudy, B. (1988). Diversity and ubiquity of K channels. *Neuroscience* **25**, 729–749.

Ruppersberg, J. P., Schroter, K. H., Sakmann, B., Stocker, M., Sewing, S. & Pongs, O. (1990). Heteromultimeric channels formed by rat brain potassium-channel proteins. *Nature* **345**, 535–537.

Saito, Y. & Isa, T. (1998). Voltage-gated transient outward currents in neurons with different firing properties in the intermediate layer of rat superior colliculus. *Society for Neuroscience Abstracts* **527**, 17.

Saito, Y. & Isa, T. (1999). Electrophysiological and morphological properties of neurons in the rat superior colliculus. I. Neurons in the intermediate layer. *Journal of Neurophysiology* **82**, 754–767.

Schwartzkroin, P. A. & Mathers, L. H. (1978). Physiological and morphological identification of a nonpyramidal hippocampal cell type. *Brain Research* **157**, 1–10.

Segal, M., Rogawski, M. A. & Barker, J. L. (1984). A transient potassium conductance regulates the excitability of cultured hippocampal and spinal neurons. *Journal of Neuroscience* **4**, 604–609.

Serôdio, P., Kentros, C. & Rudy, B. (1994). Identification of molecular components of A-type channels activating at subthreshold potentials. *Journal of Neurophysiology* **72**, 1516–1529.

Serôdio, P., Vega-Saenz de Miera, E. & Rudy, B. (1996). Cloning of a novel component of A-type K^+ channels operating at subthreshold potentials with unique expression in heart and brain. *Journal of Neurophysiology* **75**, 2174–2179.

Serrano, E. E. & Getting, P. A. (1989). Diversity of the transient outward potassium current in somata of identified molluscan neurons. *Journal of Neuroscience* **9**, 4021–4032.

Song, W.-J., Tkatch, T., Baranauskas, G., Ichinohe, N., Kitai, S. T. & Surmeier D. J. (1998). Somatodendritic depolarization-activated potassium currents in rat neostriatal cholinergic interneurons are predominantly of the A type and attributable to coexpression of Kv4·2 and Kv4·1 subunits. *Journal of Neuroscience* **18**, 3124–3137.

Storm, J. F. (1988). Temporal integration by a slowly inactivating K^+ current in hippocampal neurons. *Nature* **336**, 379–381.

Stühmer, W., Ruppersberg, J. P., Schroter, K. H., Sakmann, B., Stocker, M., Giese, K. P., Perschke, A., Baumann, A. & Pongs, O. (1989). Molecular basis of functional diversity of voltage-gated potassium channels in mammalian brain. *EMBO Journal* **8**, 3235–3244.

Surmeier, D. J., Bargas, J. & Kitai, S. T. (1989). Two types of A-current differing in voltage-dependence are expressed by neurons of the rat neostriatum. *Neuroscience Letters* **103**, 331–337.

Thompson, S. (1982). Aminopyridine block of transient potassium current. *Journal of Physiology* **80**, 1–18.

Tsaur, M. L., Chou, C. C., Shih, Y. H. & Wang, H. L. (1997). Cloning, expression and CNS distribution of Kv4.3, an A-type K^+ channel alpha subunit. *FEBS Letters* **400**, 215–220.

Tseng-Crank, J. C., Tseng, G. N., Schwartz, A. & Tanouye, M. A. (1990). Molecular cloning and functional expression of a potassium channel cDNA isolated from a rat cardiac library. *FEBS Letters* **268**, 63–68.

Wang, L.-Y., Gan, L., Forsythe, I. D. & Kaczmarek, L. K. (1998). Contribution of the Kv3.1 potassium channel to high-frequency firing in mouse auditory neurones. *Journal of Physiology* **509**, 183–194.

Warton, S. S. & Jones, D. G. (1985). Postnatal development of the superficial layers in the rat superior colliculus: a study with Golgi-Cox and Kluver-Barrera techniques. *Experimental Brain Research* **58**, 490–502.

Weiser, M., Vega-Saenz de Miera, E., Kentros, C., Moreno, H., Franzen, L., Hillman, D., Baker, H. & Rudy, B. (1994). Differential expression of Shaw-related K^+ channels in the rat central nervous system. *Journal of Neuroscience* **14**, 949–972.

Wu, R. L. & Barish, M. E. (1992). Two pharmacologically and kinetically distinct transient potassium currents in cultured embryonic mouse hippocampal neurons. *Journal of Neuroscience* **12**, 2235–2246.

Yarom, Y., Sugimori, M. & Llinás, R. (1985). Ionic currents and firing patterns of mammalian vagal motoneurons *in vitro*. *Neuroscience* **16**, 719–737.

Acknowledgements

We thank Drs Yoshihiro Kubo and Wen-Jie Song for critical reading of an earlier version of this manuscript and Michi Seo and Junko Yamamoto for technical assistance. This study was supported by Ministry of Education, Science, Sports and Culture of Japan Grant-in-Aid for Scientific Research on Priority Area (A) 10164247, Japan Society for the Promotion of Science Grant-in-Aid for Scientific Research (B) 10480232, and grants from CREST of Japan Science and Technology Corporation, the Daiko Foundation, the Naito Memorial Foundation, and the Mitsubishi Foundation (T. I.) and Japan Society for the Promotion of Science Grant-in-Aid for Encouragement of Young Scientists 11780600 (Y. S).

Corresponding author

Y. Saito: Department of Integrative Physiology, National Institute for Physiological Sciences, Myodaiji, Okazaki 444-8585, Japan.

Email: yasu@nips.ac.jp